ACS Catalysis

Research Article

pubs.acs.org/acscatalysis

Structure, Activity, and Stability of Atomically Dispersed Rh in Methane Steam Reforming

R. B. Duarte,[†] F. Krumeich,[†] and J. A. van Bokhoven*[,†,‡]

[†]Institute for Chemical and Bioengineering, ETH Zurich, 8093 Zurich, Switzerland

[‡]Paul Scherrer Institute, 5232 Villigen, Switzerland

Supporting Information

ABSTRACT: Atomically dispersed rhodium catalysts supported on xSm_2O_3–$yCeO_2$–Al_2O_3 supports were synthesized and applied in the methane steam reforming (MSR) reaction. Scanning transmission electron microscopy and MSR catalytic tests show that the dispersion of the metal, and thus the catalytic performance, depends on the support composition. The $12CeO_2$–Al_2O_3 support confers partial stability to rhodium, leading to the coexistence of atomically dispersed and nanosized rhodium particles during MSR at 773 K. A reaction mechanism with CH_4 being activated on the atomically dispersed rhodium and CO being formed on the nanoparticles is proposed. A lower rate caused by the formation of carbon species is seen in the presence of atomically dispersed rhodium and in the absence of nanoparticles as CO formation is hindered.

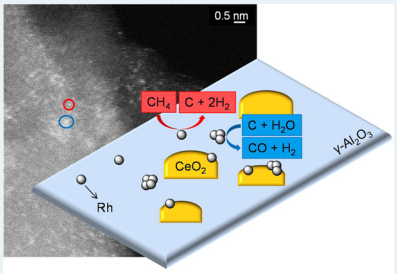

KEYWORDS: *methane steam reforming, atomically dispersed Rh catalysts, CeO_2, Sm_2O_3, scanning transmission electron microscopy, Rh/Al_2O_3-promoted catalysts*

1. INTRODUCTION

Atomic dispersion is highly desirable in heterogeneous catalytic reactions because the active sites are the surface atoms. Extensive research has been conducted on the synthesis and application of atomically dispersed heterogeneous catalysts since the work of Fu et al.,[1] who reported that the active species for the water-gas shift reaction (WGS) are atomically dispersed noble metal atoms. Qiao et al.[2] reported the synthesis of monoatomically dispersed platinum catalysts supported on iron oxide, which were successfully applied in the CO oxidation and preferential oxidation of CO in H_2. Atomically dispersed platinum catalysts are active in CO oxidation also when supported on an inert substrate, such as θ-Al_2O_3.[3] Small-load palladium catalysts applied in the selective oxidation of allylic alcohols[4] show 10-fold higher rates than a system with nanoparticle dispersion.

The methane steam reforming (MSR) reaction is important for the large scale production of H_2.[5] This reaction consists of many steps, including methane and water activation and the formation of carbon monoxide, hydrogen, and carbon dioxide.[6] Previous reports on the reaction mechanism suggest that at high temperatures (≥773 K) the dissociative CH_4 adsorption is the rate-determining step.[7−10] The activation of a C−H bond can occur on a single atom.[11] Consequently, obtaining atomically dispersed rhodium catalysts would lead to optimal catalytic performance. However, carbon monoxide is a product of the MSR reaction, and its formation is also reported to be a step that could kinetically control the reaction.[12,13] The formation of a π-bond is favored over step-edge sites, which are absent in particles less than ≈2 nm in size. The decrease in particle size might affect the carbon adsorption energy,[14] which in turn could change the reaction rates and shift the rate-determining step. Clearly, structural sensitivity has to be considered when optimizing the catalytic system.[15,16]

Ligthart et al.[10] observed an increase in the reaction rates of MSR with a decrease in the rhodium particle size to 1.3 nm. The sites that favor CO formation can be present in <2 nm particles, which interact strongly with the support. The increase in the reaction rates for methane reforming reactions with a decrease in the rhodium particle size (as small as ≈1 nm) supported on γ-Al_2O_3 has been observed many times.[7,17,18] Computational studies[19] show that at 773 K CH_4 activation will be the rate-determining step; however, nanoparticles are needed for the formation of CO with a low energy barrier, and their absence would lead to decreased reaction rates.

The use of supported noble metal catalysts for this reaction is extensively studied, and the support affects metal dispersion and stability.[7,10,20] A strong interaction between ceria and the metal phase favors the formation and stabilization of atomically dispersed atoms[1] and of small metal particles.[21,22] The addition of Sm_2O_3 to a CeO_2–Al_2O_3 support improved the activity and stability of Rh and Pt catalysts with nanoscale dispersion during MSR and methane partial oxidation, respectively.[20,23] Halabi et al.[24] proposed a mechanism for ceria−zirconia-supported rhodium catalysts, in which the formation of CO and CO_2 involves support sites or a metal−support interface. Undoubtedly revealing where steam activation proceeds is challenging, but our previous results showed that a small fraction of ceria participates in steam activation by undergoing a redox reaction.[25] Water activation involving CeO_{2-x} could

Received: October 26, 2013
Revised: March 5, 2014
Published: March 12, 2014

   dx.doi.org/10.1021/cs400979q | ACS Catal. 2014, 4, 1279−1286

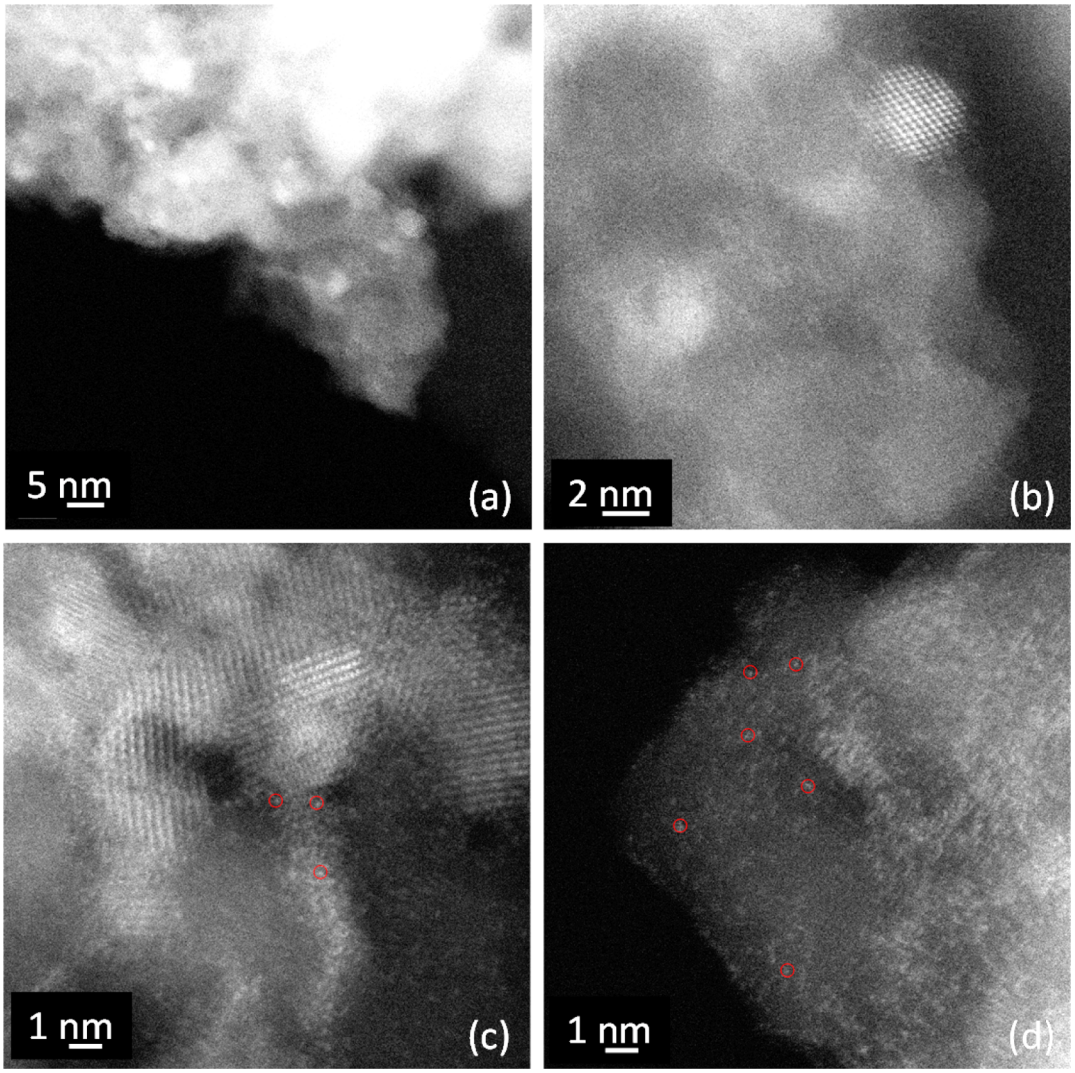

Figure 1. Representative HAADF−STEM micrographs of $12CeO_2$−Al_2O_3 (a and b) and $6Sm_2O_3$−$6CeO_2$−Al_2O_3 (c and d) supports after calcination at 773 K. Red circles mark the atomically dispersed species.

proceed on Rh, with spillover of oxygen, onto CeO_{2-x} or directly at the metal−support interface. When considering the MSR reaction mechanism and how it is affected by the metal dispersion and support composition, it is difficult to predict the performance of the catalyst. To investigate the influence of these variables, atomically dispersed rhodium catalysts supported on γ-Al_2O_3 promoted with cerium and/or samarium oxides were synthesized, characterized, and tested for MSR.

2. EXPERIMENTAL SECTION

2.1. Preparation of the Rh/$x$$Sm_2O_3$−$y$$CeO_2$−$Al_2O_3$ Catalysts. The $x$$Sm_2O_3$−$y$$CeO_2$−$Al_2O_3$ supports were prepared by wet impregnation of commercial γ-Al_2O_3 (Sigma-Aldrich) with solutions of $Sm(NO_3)_3{\cdot}6H_2O$ and/or $Ce(NO_3)_3{\cdot}6H_2O$ in ethanol.[23] The mixture was stirred at room temperature for 5 h. The ethanol was removed with a rotoevaporator at 333 K. The solids were dried and calcined at 373 K for 12 h and 773 K for 6 h, respectively. x and y are the theoretical concentrations of Sm_2O_3 and CeO_2, respectively, with values of 0, 6, and 12 wt % giving the relationship $x + y$ = 12 wt %. Catalysts were prepared according to the method of Chen et al.[26] by wet impregnation in a N_2 glovebox. An ethanol solution containing the appropriate concentration of RhOAc (Acros Organics) to obtain 0.5 wt % Rh in the final catalyst was added in $x$$Sm_2O_3$−$y$$CeO_2$-promoted or unpromoted γ-Al_2O_3. The supports were previously evacuated at 413 K for 1 h prior to being used. The mixture was stirred for 5 h followed by removal of the solvent by evacuation at 333 K. The samples were dried at 373 K overnight and then calcined at 773 K for 4 h.

2.2. Sample Characterization. Scanning transmission electron microscopy (STEM) investigations were performed on an aberration-corrected, dedicated STEM microscope, a model HD-2700CS instrument (Hitachi, 200 kV) equipped with an energy-dispersive X-ray spectrometer (EDXS) (EDAX Gemini system) for analytical investigations. The high resolution of this microscope, which is better than 0.1 nm, is due to a probe corrector (CEOS) that is incorporated in the microscope column between the condenser lens and the probe-forming objective lens.[27] Images were obtained with a high-angle annular dark-field (HAADF) detector, producing images with atomic number (Z) contrast.[28]

Temperature-programmed oxidation (TPO) measurements were performed in a CATLAB system (HIDEN Analytical) equipped with an integrated mass spectrometer. To investigate the formation of carbon species during MSR, the catalysts were

dx.doi.org/10.1021/cs400979q | ACS Catal. 2014, 4, 1279−1286

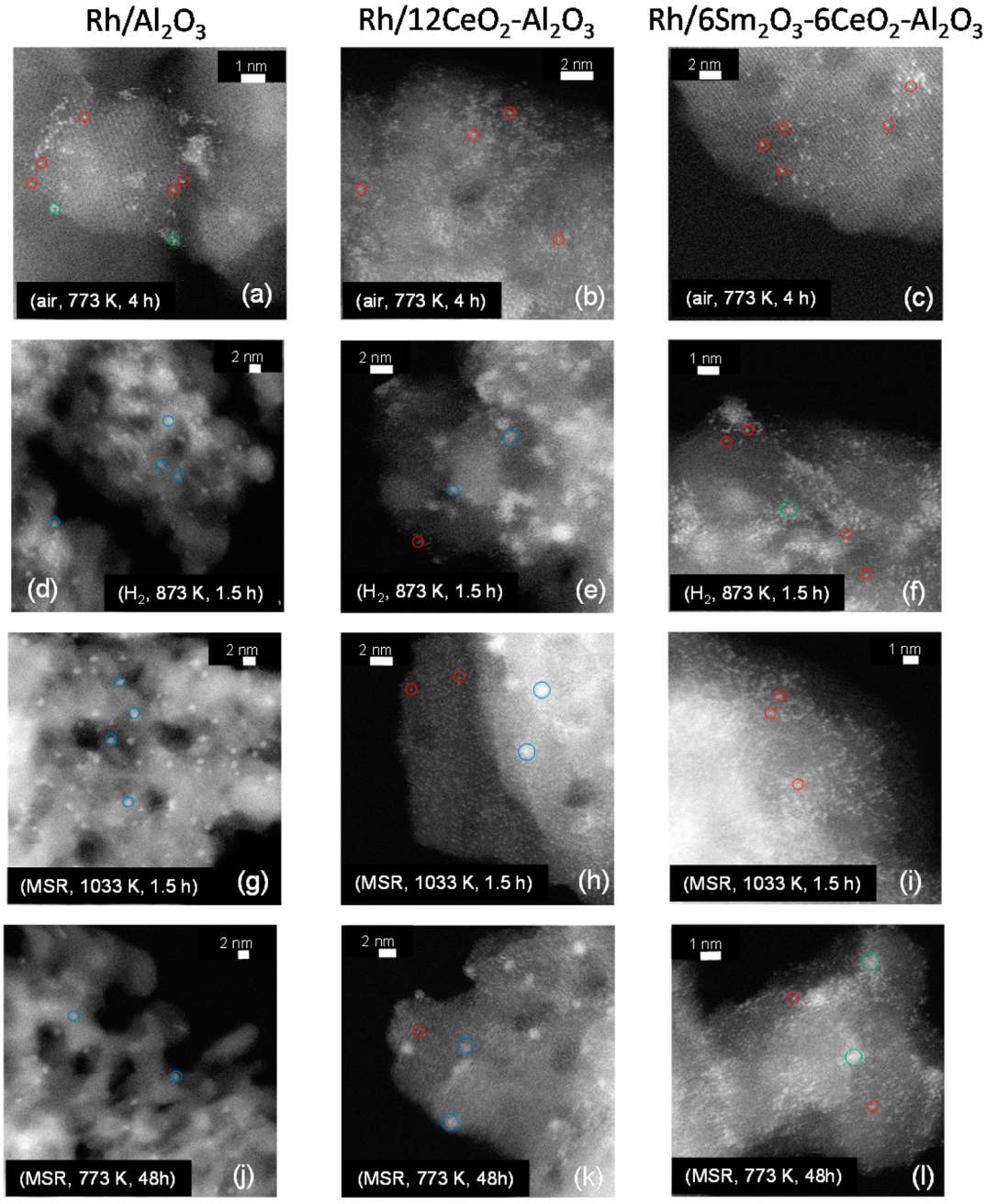

Figure 2. Representative HAADF–STEM micrographs of Rh/Al_2O_3, $Rh/12CeO_2–Al_2O_3$, and $Rh/6Sm_2O_3–6CeO_2–Al_2O_3$ catalysts after calcination at 773 K, reduction at 873 K, and MSR for 1.5 h at 1033 K, respectively, and MSR for 48 h at 773 K. Blue, green, and red circles mark the nanoparticles, clusters, and atomically dispersed rhodium, respectively.

cooled to room temperature after reaction at 773 K for 48 h and sequentially heated under a flow of a 20% O_2/He mixture to 1273 K at a rate of 10 K/min. X-ray diffraction (XRD) patterns were obtained using Cu Kα radiation and a Ni filter with an X'PERT PRO-MPD diffractometer. Diffraction peaks were recorded in a 2θ range from 10° to 70° in 0.02 intervals for 2 s. Nitrogen physisoption analyses were conducted on a Micromeritics Tristar 3000 apparatus at 77 K, and the measurements were performed after the samples had been degassed for 2 h at 473 K. The Brunauer–Emmett–Teller (BET) surface area (S_{BET}) and the average pore size diameter were calculated from the BET and the Barret–Joyner–Halenda (BJH) methods, respectively. Samples were chemically analyzed by atomic absorption spectroscopy (AAS) with a Varian SpectrAA 220 FS spectrometer, revealing a content of ≈0.5 wt % rhodium in the samples.

2.3. Catalytic Tests. Methane steam reforming reaction rates of the catalysts were measured in a CATLAB system (HIDEN Analytical) with a quartz fixed bed plug-flow reactor and an integrated mass spectrometer.[20] In the catalytic tests, 5 mg of catalyst diluted in 25 mg of γ-Al_2O_3 with a similar granulometry was used. The rates were calculated at 773 K under atmospheric pressure using a feed composition of 5% CH_4/He and steam, which was introduced into the reactor through a water saturator in a flow of helium, at a total flow rate of 540 mL/min (5 mL/min for CH_4, 15 mL/min for H_2O, and 520 mL/min for He). The stability of the catalysts was tested for 48 h. The gas composition at the outlet was recorded by the

dx.doi.org/10.1021/cs400979q | ACS Catal. 2014, 4, 1279–1286

mass spectrometer (current vs time). The conversion was calculated from mass spectrometry analysis, and the rate of methane consumption was determined on the basis of the methane inlet flow. Reaction rates were calculated in differential mode on the basis of the fact that the MSR reaction is zero-order in H_2O and first-order in CH_4, and assuming uniform catalytic properties throughout the bed.[20] The forward CH_4 turnover rates (r_f) were calculated by correction of the net reaction rate (r_n) for the approach to thermodynamic equilibrium (η)[7,29] by

$$r_n = r_f(1 - \eta) \quad (1)$$

with

$$\eta = \frac{P_{CO}P_{H_2}{}^3}{P_{CH_4}P_{H_2O}}\frac{1}{K_{eq}} \quad (2)$$

The corrections were minor, and the rate of reforming becomes[7,10]

$$r_f = kP_{CH_4} \quad (3)$$

Mass and heat transfer limitations on the reactor scale were ruled out by changing the dilution ratio. Intraparticle and extraparticle limitation were excluded by examination of rates from catalytic tests with varied particle sizes and by tests in which the flow rate was varied and the space time kept constant, respectively.[30,31]

The reaction rates were normalized per surface atom assuming that the reaction proceeds on all rhodium surface sites. The dispersion can be estimated from the particle size[32] obtained from the HAADF−STEM micrographs of the catalysts after 48 h in MSR at 773 K. The assessment of the dispersion was done by the analysis of many images. The average number of surface atoms in the catalysts containing both nanoparticles and atomically dispersed rhodium was calculated by counting the individual atoms in a fixed area and correlating to the number of atoms in nanoparticles in an equally large area. A rough estimate indicates atomic dispersion of ∼50% in the CeO_2-promoted catalyst.

3. RESULTS

3.1. Atomically Dispersed Rhodium and Rhodium Nanoparticles. Figure 1 shows HAADF−STEM micrographs of supports $12CeO_2$−Al_2O_3 (a and b) and $6Sm_2O$−-$6CeO_2$−Al_2O_3 (c and d) after calcination at 773 K. The bright spots correspond to cerium and samarium oxide particles, while the large gray areas are the alumina. The determination of the particle size distribution in the ceria-containing support is difficult because individual particles are hard to distinguish; however, the well-separated particles are between ∼2.5 and ∼4.2 nm in size. The support containing both promoters has, besides the larger particles, very small clusters and atomically dispersed species (red circles). Because ceria-containing alumina (Figure 1a,b) shows no atomically dispersed species, those observed in the $6Sm_2O_3$−$6CeO_2$−Al_2O_3 sample (Figure 1c,d) are likely samarium atoms.

Figure 2 shows representative HAADF−STEM micrographs of Rh/Al_2O_3, $Rh/12CeO_2$−Al_2O_3, and $Rh/6Sm_2O_3$−$6CeO_2$−Al_2O_3 catalysts after calcination at 773 K, reduction at 873 K, and MSR for 1.5 h at 1033 K, respectively, and MSR for 48 h at 773 K. In these images, rhodium appears as bright dots. However, it is difficult to achieve a clear and unambiguous distinction among rhodium, cerium, and samarium because they appear with similar brightnesses in the Z contrast micrographs because of the relatively small differences in their atomic numbers (Z_{Rh} = 45, Z_{Ce} = 58, and Z_{Sm} = 62). The large bright patches, very often with distinguishable lattice fringes, correspond to ceria nanocrystals (Figure S1 of the Supporting Information). Atomically dispersed rhodium is observed in all samples after calcination (Figure 2a−c and Table 1). The promoted catalysts have exclusively atomically dispersed rhodium (red circles), while the Rh/Al_2O_3 catalyst also contains small clusters (green circles) between 0.3 and 1.1 nm in size. The XRD patterns of the supports and catalysts (Figure S2 of the Supporting Information) show diffraction peaks of γ-Al_2O_3 (2θ values of 33.6°, 37.5°, 39.4°, 45.6°, and 67.4°), and the samples containing promoters also show reflections characteristic of ceria with a fluorite-type structure (2θ values of 28.6°, 33.3°, 47.4°, and 56.5°). Peaks of samarium oxide are not observed, suggesting that samarium species are highly dispersed, in good agreement with the STEM micrographs of the support (Figure 1). The textural properties and structure of the support remain practically unchanged after the impregnation with rhodium acetate and calcination at 773 K (Table S1 and Figure S2 of the Supporting Information).

Table 1. Particle Size Distribution Based on STEM Micrographs Taken after Different Thermal Treatments under Different Atmospheres

		dispersion based on TEM	
sample	treatment	atomically dispersed Rh	Rh particle size (nm)
Rh/Al_2O_3	air, 773 K, 4 h	yes	0.3−1.1
	H_2, 873 K, 1.5 h	no	0.5−1.7
	MSR, 1033 K, 1.5 h	no	0.5−2.1
	MSR, 773 K, 48 h	no	0.9−1.9
$Rh/12CeO_2$−Al_2O_3	air, 773 K, 4 h	yes	–
	H_2, 873 K, 1.5 h	yes	0.5−2.3
	MSR, 1033 K, 1.5 h	yes	0.9−1.9
	MSR, 773 K, 48 h	yes	0.5−2.3
$Rh/6Sm_2O_3$−$6CeO_2$−Al_2O_3	air, 773 K, 4 h	yes	–
	H_2, 873 K, 1.5 h	yes	0.3−1.3
	MSR, 1033 K, 1.5 h	yes	0.8−2.3
	MSR, 773 K, 48 h	yes	≤1

After reduction at 873 K, the Rh/Al_2O_3 catalyst (Figure 2d) shows nanoparticles (blue circles) between 0.5 and 1.7 nm in size and atomically dispersed rhodium is not recognizable. The catalyst promoted by ceria (Figure 2e) still shows atomically dispersed rhodium (red circles), but to a reduced extent, and nanoparticles (blue circles) between 0.5 and 2.3 nm in size. The catalyst containing both oxide promoters (Figure 2f) contains mainly atomically dispersed rhodium (red circles) with very few small clusters between 0.3 and 1.3 nm in size (green circles). After MSR at 1033 K, all samples show significant sintering. Rh/Al_2O_3 (Figure 2g) no longer shows atomically dispersed rhodium, and the high-temperature reaction leads to the formation of nanoparticles (blue circles) between 0.5 and 2.1 nm in size. Both promoted samples (Figure 2h,i) show fewer changes, maintaining partially the atomic dispersion (red

dx.doi.org/10.1021/cs400979q | ACS Catal. 2014, 4, 1279−1286

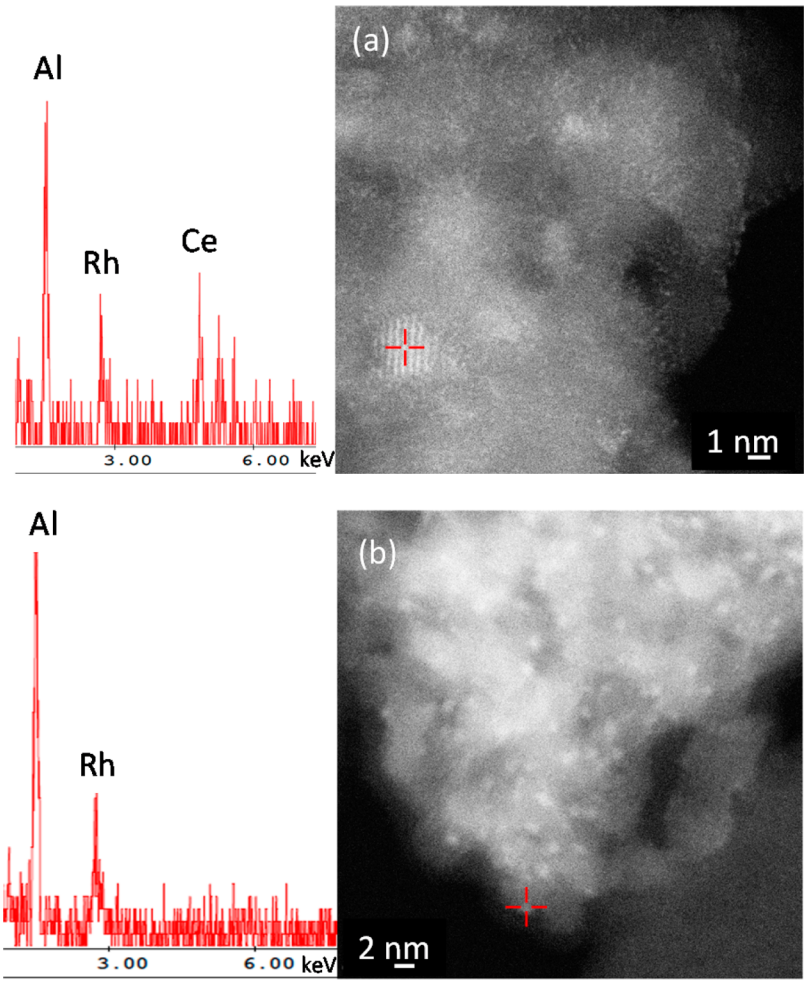

Figure 3. EDXS spot analysis and HAADF−STEM micrographs of Rh/12CeO_2−Al_2O_3 after MSR for 48 h at 773 K. The positions analyzed are specified in the STEM micrographs.

circles) while also forming a significant fraction of nanoparticles (blue circles) of roughly the same size (between ≈0.8 and 2.3 nm). The sample containing samarium oxide shows a very high stability of the metal phase after reduction at 873 K (Figure 2f), but it sinters considerably at higher temperatures (Figure S3 of the Supporting Information). HAADF−STEM imaging combined with EDXS analysis shows that the sintering of samarium particles also happens after reduction at 873 K and MSR at 1033 K, as it is detected in the bright areas of the micrographs (Figure S4 of the Supporting Information). This indicates that sintering of samarium is more severe than that of rhodium, because rhodium could not be detected in the very small particles in those areas.

The MSR stability test carried for 48 h leads to sintering of the nonpromoted sample: the particles show an increase of their average size from 1.1 nm after calcination to 1.9 nm after MSR at 773 K (Figure 2j). Rhodium in the ceria-containing sample (Figure 2k) sinters partly during the reaction and nanoparticles (blue circles) are present with a broad size range between 0.5 and 2.3 nm. Examination of different regions of the Rh/6Sm_2O_3-6CeO_2−Al_2O_3 catalyst (Figure 2l) reveals that mainly atomically dispersed rhodium (red circles) is present and very few clusters (green circles) with a diameter up to 1 nm are observed.

Figure 3 shows the STEM micrographs of Rh/12CeO_2−Al_2O_3 after the 48 h MSR stability test at 773 K and the EDXS spot analysis of the two specified positions. The EDX spectrum (a) shows peaks attributed to aluminum, cerium, and rhodium. The area that appears to be bright is thus a CeO_2 crystal located on the support that is coated by finely dispersed Rh. The HAADF−STEM image (b) confirms the occurrence of partial sintering during the 48 h MSR catalytic test in the Rh/12CeO_2−Al_2O_3 catalyst, which shows rhodium particles as bright spots between 0.5 and 2.3 nm in size, as confirmed by EDX spectroscopy analysis of such a spot.

3.2. Catalytic Performance. Table 2 lists the rates of the catalysts for the MSR reaction after 1 and 48 h at 773 K and the percentage of deactivation during this period. Rh/Al_2O_3 has the lowest rate with an initial value of 1.5 molecules $site^{-1}$ s^{-1}, decreasing to 0.9 molecule $site^{-1}$ s^{-1} after 48 h under a stream, showing a deactivation of 40%. The ceria-promoted catalyst

Table 2. Reaction Rates of the Catalysts after 1 and 48 h in MSR at 773 K and Deactivation during the Test

	reaction rate (no. of molecules $site^{-1}$ s^{-1})		
sample	1 h	48 h	deactivation (%)
Rh/Al_2O_3	1.5	0.9	40
Rh/12CeO_2−Al_2O_3	2.3	1.9	17
Rh/6Sm_2O_3−6CeO_2−Al_2O_3	1.8	1.2	33

dx.doi.org/10.1021/cs400979q | *ACS Catal.* 2014, 4, 1279−1286

shows the highest rates of 2.3 and 1.9 molecules site^{-1} s^{-1} after 1 and 48 h, respectively. Rh/12CeO_2−Al_2O_3 shows a 17% lower level of deactivation after 48 h. The rates for Rh/6Sm_2O_3−6CeO_2−Al_2O_3 are 1.8 and 1.2 molecules site^{-1} s^{-1} after 1 and 48 h, respectively, which corresponds to 33% deactivation.

Figure 4 shows the carbon dioxide production during TPO experiments, which were performed after MSR for 48 h at 773 K to determine whether the observed deactivation may be due to the formation of carbon species. Carbon dioxide release is observed around 380 K and between 500 and 700 K for all samples. The peaks at lower temperatures probably are related to the desorption of CO_2 chemisorbed on the catalyst surface during the reforming reaction.[33] The Rh/6CeO_2−6Sm_2O_3−Al_2O_3 catalyst additionally shows CO_2 release at 1080 K, possibly because of the oxidation of some kinds of carbon species strongly bound to the surface. Only this catalyst forms such species.

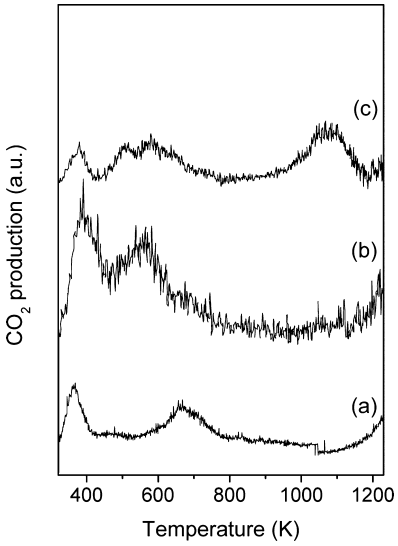

Figure 4. Carbon dioxide production during TPO of the (a) Rh/Al_2O_3, (b) Rh/12CeO_2−Al_2O_3, and (c) Rh/6CeO_2−6Sm_2O_3−Al_2O_3 catalysts after MSR for 48 h at 773 K in a 20% O_2/He mixture.

4. DISCUSSION

Atomically dispersed rhodium catalysts were successfully synthesized on promoted and nonpromoted alumina. The efficient synthesis of Rh/Al_2O_3 catalysts with atomically dispersed rhodium was previously reported,[26] in which the structure remained stable with heating under vacuum until the temperature reached nearly 800 K. However, the stability of the dispersed rhodium atoms is a function of the support composition, temperature, and environment. Sintering occurs after the different thermal treatments to varied extents in all samples, and the absence of promoters led to more severe sintering. CeO_2-containing supports partially keep the rhodium atomically dispersed. Ceria favors the formation and stabilization of atomically dispersed metal species and small metal particles due to a strong metal−support interaction.[1,21,22,34] Figure 3 shows through EDXS spot analysis that part of the rhodium is in close contact with ceria. The stabilization of metal particles was reported to be due to the formation of a metal−O−Ce bond,[35] which acts as an anchor and inhibits metal mobility. However, STEM micrographs (Figure 2e,h,k) show that atomically dispersed rhodium is also sitting on alumina. It was observed in our previous work[20] that the presence of ceria as a promoter in Rh/Al_2O_3 catalysts inhibits alumina surface area loss after MSR reaction at 1033 K. Prior results[25] of *in situ* XAS measurements and XRD analysis suggest that with heating to 773 K under MSR conditions a part of the cerium is incorporated into the alumina structure as highly dispersed species forming $CeAlO_3$, which stabilizes alumina. Pt/Al_2O_3 catalysts were reported[36] to have improved stability because of the stabilization of alumina by WO_x, which is extended to PtO_x species. The 6Sm_2O_3−6CeO_2−Al_2O_3 support maintains the highest level of dispersion: very few clusters are observed after reduction at 873 K and MSR at 773 K. The same support proved to be very efficient in the stabilization of rhodium nanoparticles during MSR,[20] and it yielded a high degree of dispersion for Pt nanoparticles compared to that with the CeO_2−Al_2O_3 support.[23] Figure 1 shows that samarium is present as clusters and atomically dispersed species in the support after calcination at 773 K. Wang et al.[37] observed that the presence of lanthanum atoms adsorbed on the surface of alumina inhibits its sintering, proving that highly dispersed dopants are effective in support stabilization.

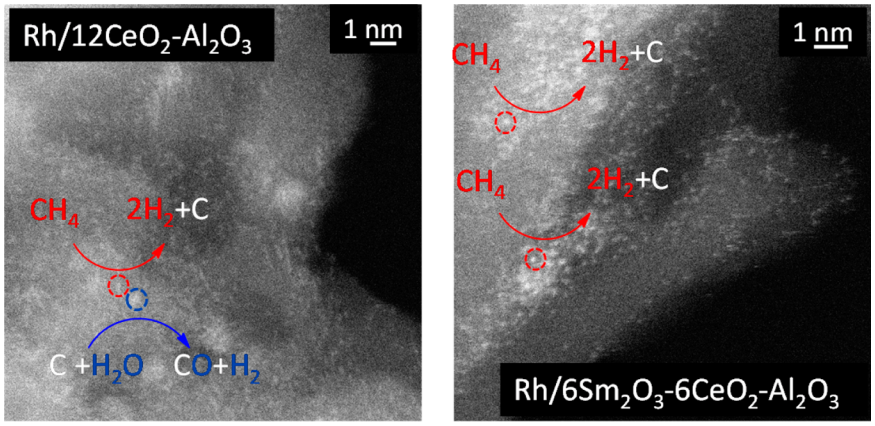

Figure 5. Mechanism proposed on the basis of STEM, TPO, and catalytic results. Methane activation on atomically dispersed rhodium species leads to the formation of carbon, which becomes oxidized on adjacent nanoparticles in the Rh/12CeO_2−Al_2O_3 sample. Because of the absence of rhodium nanoparticles in the Rh/6Sm_2O_3−6CeO_2−Al_2O_3 catalyst, CO formation is hindered and some kinds of carbon species strongly bound to the surface form as a result.

dx.doi.org/10.1021/cs400979q | *ACS Catal.* 2014, 4, 1279−1286

The atomically dispersed rhodium catalysts do not need any reductive activation to show catalytic activity in the MSR reaction, and the reaction rates are comparable to those reported previously in the literature for rhodium catalysts.[7,10,20]

The elementary steps, which were considered as candidates to kinetically control the MSR reaction, are methane activation and CO formation.[7−10,12,13] The rate of methane activation is expected to increase with a decrease in particle size (from nanoparticles to atoms). CO recombination, however, presents a lower energy barrier over stepped surfaces, which are present in nanoparticles ∼2 nm in diameter.[10,38] The coexistence of rhodium in the form of dispersed atoms and nanoparticles would thus lead to the formation of an optimal system for the reaction. The $Rh/12CeO_2−Al_2O_3$ catalyst shows the best performance, and the STEM images of this catalyst suggest that this is due to stabilization of atomically dispersed and small rhodium nanoparticles. Figure 5 shows a proposed mechanism in which we assume that carbon originating from methane dissociative adsorption on atomically dispersed rhodium forms subsequently CO on an adjacent rhodium nanoparticle. Migration of carbon on supported metal catalysts was previously reported for Pt, Co, and Pt−Re catalysts supported on alumina.[39−41] Carbon likely migrates from rhodium atoms and/or nanoparticles to the support.[39−41] The mobility of such species may result in oxidation of these carbon species on rhodium nanoparticles. The samaria-containing promoted catalyst shows a lower reaction rate and a decreased stability during MSR compared to those of the $Rh/12CeO_2−Al_2O_3$ catalyst. A possible reason for its inferior performance is the deposition of carbon species: this sample also shows very few nanoparticles after MSR at 773 K for 48 h and, therefore, a lack of step-edge sites.[10] This would hinder the oxidation of the carbon coming from activated methane, thus leading to formation of the carbon species observed in the TPO at 1080 K (Figure 4). According to the STEM micrographs of the catalysts after MSR at 1033 K (Figure S3 of the Supporting Information), such a high temperature would lead to sintering of rhodium, which consequently created step-edge sites that facilitate the oxidation of those species.

A straight correlation between dispersion and reaction rates in MSR has been observed many times.[7−10,12] The Rh/Al_2O_3 catalyst shows the lowest reaction rate and the highest level of deactivation during the 48 h MSR reaction. According to STEM images, this nonpromoted catalyst is also the one that shows the strongest sintering after the different treatments. The inferior performance of this catalyst is related to the inability of the support to stabilize the rhodium dispersion during reaction. Rhodium catalysts with initial nanosized rhodium particles[20] undergo sintering of the metal phase as the main reason for deactivation during MSR. Therefore, sintering is very likely the reason for the lowered reaction rate and observed deactivation in the Rh/Al_2O_3 catalyst. Ligthart et al.[10] reported that oxidation of small rhodium particles is the reason of the deactivation observed during MSR. Our previous study[20] shows that under both MSR and a reductive atmosphere, rhodium nanoparticles are completely reduced. X-ray absorption near-edge structure measurements at the Rh K-edge of the catalysts under a reductive atmosphere at 773 K (Figure S5 of the Supporting Information) show that the spectra of all three catalysts are similar and show features of only the rhodium-reduced state, ruling out different electronic states of rhodium under a reductive atmosphere, such as the MSR.

5. CONCLUSION

Promoted catalysts show higher stability of atomically dispersed and of nanosized rhodium particles during MSR at 773 K. The $Rh/12CeO_2−Al_2O_3$ catalyst shows the best performance in the reaction. STEM micrographs of this catalyst show the existence of both atomically dispersed and rhodium nanoparticles. The $Rh/6Sm_2O_3−6CeO_2−Al_2O_3$ catalyst, which shows mainly atomically dispersed rhodium after MSR at 773 K, shows lowered rates and stronger deactivation because of the formation of carbon species. These observations suggest the occurrence of a mechanism in which methane activation occurring on the atomically dispersed rhodium will lead to the formation of carbon, which will be oxidized with the aid of nanoparticles. The absence of nanoparticles in the $Rh/6Sm_2O_3−6CeO_2−Al_2O_3$ catalyst hinders CO formation and leads to a decreased rate because of the formation of carbon species strongly bound to the surface.

■ ASSOCIATED CONTENT

Supporting Information

Textural properties and XRD analysis of the supports and catalysts and additional representative HAADF−STEM micrographs and EDXS spot analysis of the catalysts. This material is available free of charge via the Internet at http://pubs.acs.org.

■ AUTHOR INFORMATION

Corresponding Author

*ETH Zurich, Chemistry and Bioengineering, HCI E 127, Wolfgang-Paulistr. 10, 8093 Zürich, Switzerland. Phone: +41 44 632 55 42. E-mail: jeroen.vanbokhoven@chem.ethz.ch.

Notes

The authors declare no competing financial interest.

■ ACKNOWLEDGMENTS

We thank the electron microscopy center of ETH Zurich (EMEZ) for providing measurement time.

■ REFERENCES

(1) Fu, Q.; Saltsburg, H.; Flytzani-Stephanopoulos, M. *Science* **2003**, *301*, 935.
(2) Qiao, B. T.; Wang, A. Q.; Yang, X. F.; Allard, L. F.; Jiang, Z.; Cui, Y. T.; Liu, J. Y.; Li, J.; Zhang, T. *Nat. Chem.* **2011**, *3*, 634.
(3) Moses-DeBusk, M.; Yoon, M.; Allard, L. F.; Mullins, D. R.; Wu, Z.; Yang, X.; Veith, G.; Stocks, G. M.; Narula, C. K. *J. Am. Chem. Soc.* **2013**, *135*, 12634.
(4) Hackett, S. E. J.; Brydson, R. M.; Gass, M. H.; Harvey, I.; Newman, A. D.; Wilson, K.; Lee, A. F. *Angew. Chem., Int. Ed.* **2007**, *46*, 8593.
(5) McFarland, E. *Science* **2012**, *338*, 340.
(6) Xu, J. G.; Froment, G. F. *AIChE J.* **1989**, *35*, 88.
(7) Wei, J. M.; Iglesia, E. *J. Catal.* **2004**, *225*, 116.
(8) Wei, J. M.; Iglesia, E. *Phys. Chem. Chem. Phys.* **2004**, *6*, 3754.
(9) Wei, J. M.; Iglesia, E. *J. Phys. Chem. B* **2004**, *108*, 4094.
(10) Ligthart, D. A. J. M.; van Santen, R. A.; Hensen, E. J. M. *J. Catal.* **2011**, *280*, 206.
(11) Van Santen, R. A. *Acc. Chem. Res.* **2009**, *42*, 57.
(12) Jones, G.; Jakobsen, J. G.; Shim, S. S.; Kleis, J.; Andersson, M. P.; Rossmeisl, J.; Abild-Pedersen, F.; Bligaard, T.; Helveg, S.; Hinnemann, B.; Rostrup-Nielsen, J. R.; Chorkendorff, I.; Sehested, J.; Norskov, J. K. *J. Catal.* **2008**, *259*, 147.
(13) Halabi, M. H.; de Croon, M. H. J. M.; van der Schaaf, J.; Cobden, P. D.; Schouten, J. C. *Appl. Catal., A* **2010**, *389*, 80.
(14) Norskov, J. K.; Bligaard, T.; Kleis, J. *Science* **2009**, *324*, 1655.
(15) Boudart, M. *Adv. Catal.* **1969**, *20*, 153.

(16) Guthrie, W. L.; Sokol, J. D.; Somorjai, G. A. *Surf. Sci.* **1981**, *109*, 390.
(17) Zhang, Z. L.; Tsipouriari, V. A.; Efstathiou, A. M.; Verykios, X. E. *J. Catal.* **1996**, *158*, 51.
(18) Wang, H. Y.; Ruckenstein, E. *Appl. Catal., A* **2000**, *204*, 143.
(19) Zhu, T. W.; van Grootel, P. W.; Filot, I. A. W.; Sun, S. G.; van Santen, R. A.; Hensen, E. J. M. *J. Catal.* **2013**, *297*, 227.
(20) Duarte, R. B.; Nachtegaal, M.; Bueno, J. M. C.; van Bokhoven, J. A. *J. Catal.* **2012**, *296*, 86.
(21) Kundakovic, L.; Flytzani-Stephanopoulos, M. *J. Catal.* **1998**, *179*, 203.
(22) Farmer, J. A.; Campbell, C. T. *Science* **2010**, *329*, 933.
(23) Duarte, R. B.; Damyanova, S.; de Oliveira, D. C.; Marques, C. M. P.; Bueno, J. M. C. *Appl. Catal., A* **2011**, *399*, 134.
(24) Halabi, M. H.; de Croon, M. H. J. M.; van der Schaaf, J.; Cobden, P. D.; Schouten, J. C. *Appl. Catal., A* **2010**, *389*, 68.
(25) Duarte, R. B.; Safonova, O. V.; Krumeich, F.; Makosch, M.; van Bokhoven, J. A. *ACS Catal.* **2013**, *3*, 1956.
(26) Chen, Z.; Chun, W.; Fukui, K. *Photon Factory Activity Report*; Photon Factory: Tsukuba, Japan, 2010; Vol. *27*.
(27) Inada, H.; Wu, L. J.; Wall, J.; Su, D.; Zhu, Y. M. *J. Electron Microsc.* **2009**, *58*, 111.
(28) Pennycook, S. J. *Ultramicroscopy* **2012**, *123*, 28.
(29) Hou, K. H.; Hughes, R. *Chem. Eng. J.* **2001**, *82*, 311.
(30) Koros, R. M.; Nowak, E. J. *Chem. Eng. Sci.* **1967**, *22*, 470.
(31) Boudart, M. *Chem. Rev.* **1995**, *95*, 661.
(32) de Graaf, J.; van Dillen, A. J.; de Jong, K. P.; Koningsberger, D. C. *J. Catal.* **2001**, *203*, 307.
(33) Zheng, J.; Song, C.; Pan, W.; Sun, L.; Nataraj, S.; Wilhelm, F.; Armor, J. N. *Prepr. Pap.—Am. Chem. Soc., Div. Fuel Chem.* **2003**, *48*, 801.
(34) Kalakkad, D.; Datye, A. K.; Robota, H. *Appl. Catal., B* **1992**, *1*, 191.
(35) Nagai, Y.; Hirabayashi, T.; Dohmae, K.; Takagi, N.; Minami, T.; Shinjoh, H.; Matsumoto, S. *J. Catal.* **2006**, *242*, 103.
(36) Contreras, J. L.; Fuentes, G. A. *11th International Congress on Catalysis: 40th Anniversary, Parts A and B*; Elsevier Science Publishing Co.: Amsterdam, 1996; Vol. *101*, p 1195.
(37) Wang, S. W.; Borisevich, A. Y.; Rashkeev, S. N.; Glazoff, M. V.; Sohlberg, K.; Pennycook, S. J.; Pantelides, S. T. *Nat. Mater.* **2004**, *3*, 274.
(38) van Grootel, P. W.; Hensen, E. J. M.; van Santen, R. A. *Langmuir* **2010**, *26*, 16339.
(39) Myers, C. G.; Lang, W. H.; Weisz, P. B. *Ind. Eng. Chem.* **1961**, *53*, 299.
(40) Boskovic, G.; Smith, K. J. *Catal. Today* **1997**, *37*, 25.
(41) Sanchez, S. I.; Moser, M. D.; Bradley, S. A. *ACS Catal.* **2014**, *4*, 220.